AGU PUBLICATIONS

Geophysical Research Letters

RESEARCH LETTER
10.1002/2017GL072883

Key Points:
- A new model to estimate the amount of air entrained by breaking waves in the open ocean
- Combines a breaking wave model with field data of breaking statistics to present relationships between oceanic variables and air entrainment
- Implications for gas transfer parameterization

Correspondence to:
L. Deike,
ldeike@princeton.edu

Citation:
Deike, L., L. Lenain, and W. K. Melville (2017), Air entrainment by breaking waves, *Geophys. Res. Lett.*, *44*, 3779–3787, doi:10.1002/2017GL072883.

Received 31 JAN 2017
Accepted 5 APR 2017
Accepted article online 17 APR 2017
Published online 24 APR 2017

Air entrainment by breaking waves

Luc Deike[1,2,3], Luc Lenain[3], and W. Kendall Melville[3]

[1]Department of Mechanical and Aerospace Engineering, Princeton University, Princeton, New Jersey, USA, [2]Princeton Environmental Institute, Princeton University, Princeton, New Jersey, USA, [3]Scripps Institution of Oceanography, University of California San Diego, La Jolla, California, USA

Abstract We present an estimate of the total volume of entrained air by breaking waves in the open ocean, based on a model for a single breaking wave and the statistics of breaking waves measured in the field and described by the average length of breaking crests moving with speeds in the range $(c, c + \mathrm{d}c)$ per unit area of ocean surface, $\Lambda(c)\mathrm{d}c$, introduced by Phillips (1985). By extending the single breaking wave model to the open ocean, we show that the volume flux of air entrained by breaking waves, V_A (volume per unit ocean area per unit time, a velocity), is given by the third moment of $\Lambda(c)$, modulated by a function of the wave slope. Using field measurements of the distribution $\Lambda(c)$ and the wave spectrum, we obtain an estimate of the total volume flux of air entrained by breaking for a wide range of wind and wave conditions. These results pave the way for accurate remote sensing of the air entrained by breaking waves and subsequent estimates of the associated gas transfer.

Plain Language Summary Processes at the ocean-atmosphere interface control the transfer of gas and have a profound effect on weather and climate. Among these processes, breaking waves play an important role by entraining bubbles into the ocean. The dynamics and statistics of breaking waves in a particular location of the ocean are complex and depend mainly on the local sea state and not only the wind speed. However, current parameterizations of air-sea gas transfer rely solely on the wind speed, which leads to large uncertainties in the air-sea exchange budget of gases key to the climate system. In this paper, we present a theoretical model to estimate the volume of air entrained in the ocean by breaking waves. Using our model and field measurements of the wave and wave breaking statistics, we obtain an estimate of the total volume of air entrained by breaking for a wide range of wind and wave conditions. These results pave the way for accurate remote sensing of the air entrained by breaking waves and estimates of the associated gas transfer, which will lead to improvements in current climate models.

1. Introduction

Processes at the ocean-atmosphere interface control the transfer of gas and have therefore a profound effect on weather and climate [*Melville*, 1996; *de Leeuw et al.*, 2011; *Garbe et al.*, 2014; *Veron*, 2015]. Among these processes, deep water breaking waves play an important role by entraining bubbles into the ocean. The dynamics and statistics of breaking waves in a particular location of the ocean are complex and depend primarily on the local sea state not the wind speed.

However, current parameterizations of air-sea gas transfer rely solely on the wind speed. Recent gas transfer measurements in the ocean, using eddy covariance techniques, have shown large scatter in the gas transfer velocity, when analyzed as a function of wind speed only, for gases key to the climate system, such as O_2, CO_2, and dimethyl sulfide [*Garbe et al.*, 2014]. This demonstrates the failure of wind speed parameterization at moderate to high wind speeds where it is expected that the role of bubble-mediated gas transfer due to air entrainment by breaking waves will become more important.

The role of bubbles in air-sea gas transfer has been the subject of numerous studies, demonstrating their importance [*Wallace and Wirick*, 1992; *Keeling*, 1993; *Liang et al.*, 2012, 2013], separating the contribution to the total flux into the transfer of gas due to bubbles entrained by breaking waves and the diffusive transfer at an unbroken interface. However, the complex nature of breaking and air entrainment, a two-phase turbulent process, has made a priori quantification of the bubble statistics a challenging task. Recently, combining laboratory data and novel numerical simulations, *Deike et al.* [2016] proposed a consistent and predictive model

for the amount of air entrained by breaking and the associated bubble statistics, as a function of the input wave variables. It showed a linear relation between air entrainment and mechanical energy dissipated by breaking waves. Combining this model with recent measurements of the breaking statistics, we propose a formulation for the volume flux of air entrained in the ocean by breaking waves. This represents a first step in improving and rationalizing the role of bubbles entrained by breaking waves in the total gas transfer from the atmosphere to the ocean.

Breaking statistics in the field are described by the distribution of the average breaker front length, $\Lambda(c)$, per unit area of sea surface per unit increment of breaking front velocity c, first introduced by *Phillips* [1985]. The moments of $\Lambda(c)$ have important physical interpretations [*Phillips*, 1985]. The first and second moments are related to the frequency of breaking and whitecap coverage, i.e., the fraction of ocean surface area turned over by breaking fronts. The fourth moment is related to the momentum flux from the wavefield to the upper ocean $\mathbf{F}_m = (\rho/g)\int b\mathbf{c}c^3\Lambda(\mathbf{c})\mathrm{d}\mathbf{c}$, where g is gravity, ρ is the water density, and b is the nondimensional breaking strength. The fifth moment gives the total gravity wave energy dissipated by breaking waves per unit area of ocean surface $S_{\mathrm{diss}} = (\rho/g)\int bc^5\Lambda(c)\mathrm{d}c$. Extensive laboratory measurement of unsteady breaking waves has shown that the breaking strength, b, varies with the wave slope. *Drazen et al.* [2008] proposed an inertial scaling argument based on a classical turbulence result of *Taylor* [1935] that relates b to the slope at breaking $S = hk$, $b \propto S^{5/2}$, where h is a measure of the height of the breaking wave and k the characteristic wave number. Introducing a breaking threshold, *Romero et al.* [2012] showed that to leading order, $b = 0.4(S - 0.08)^{5/2}$ described all available laboratory data, from incipient to plunging breakers. Recent numerical and experimental work has further confirmed [*Grare et al.*, 2013; *Deike et al.*, 2015, 2016; *Derakhti and Kirby*, 2016] and extended these results to parasitic capillaries [*Melville and Fedorov*, 2015; *Deike et al.*, 2015]. *Romero et al.* [2012] used the inertial model to develop a semiempirical spectral model of the breaking parameter b and breaking dissipation in the field. By measuring the dissipation in the ocean surface layer using acoustic Doppler and infrared sensors, *Sutherland and Melville* [2013, 2015] managed to close the wave breaking energy budget using the fifth moment of $\Lambda(c)$ and the formulation from *Romero et al.* [2012]. This demonstrates the ability to measure properties of the upper ocean, such as energy dissipation due to breaking, through remote sensing of the wavefield and the breaking statistics.

Here we follow a similar strategy to estimate the amount of air entrained by breaking waves. By extending to the open ocean the model for a single breaking wave presented in *Deike et al.* [2016], we show that the third moment of $\Lambda(c)$, modulated by a function of the wave slope, gives the volume of entrained air by breaking waves, per unit time, per unit area of ocean surface, V_A. Using this formulation, we estimate the volume flux of air entrained by breaking waves, V_A, using field measurements of the wave and breaking statistics, previously described in the literature [*Kleiss and Melville*, 2010; *Romero and Melville*, 2010; *Sutherland and Melville*, 2013; *Lenain and Melville*, 2017], and discuss its relationship to meteorological and wave state variables.

2. A Model for the Entrainment of Air by Breaking Waves in the Field

We recall the model from *Deike et al.* [2016] for a single breaking wave and extend this formulation to the open ocean, described by the statistics of breaking given by $\Lambda(c)$ and the statistics of the waves described by the wave spectrum.

2.1. Air Entrainment by a Single Breaking Wave

In *Deike et al.* [2016], we presented a model to describe the air entrained and the bubble statistics by a single breaking wave, based on the geometry of the entrained bubble cloud, a balance between buoyancy forces and viscous dissipation when entraining the bubbles, and turbulent fragmentation. The model, based on physical arguments, describes correctly the limited available laboratory data [*Lamarre and Melville*, 1991; *Duncan*, 1981; *Deane and Stokes*, 2002; *Lim et al.*, 2015] and our direct numerical simulations (DNSs) [*Deike et al.*, 2016] of air entrainment and bubble statistics entrained by breaking waves.

The bubble size distribution, $N(r,t)$, over the total volume of breaking, $V_0 = AL_c = \pi h^2/4L_c$, where h is the height of the breaker and L_c the length of breaking crest, is given by [*Deike et al.*, 2016]

$$N(r,t) = B\frac{AL_c}{2\pi}\frac{\varepsilon(t-\Delta\tau)}{Wg}r^{-10/3}r_m^{-2/3}, \tag{1}$$

where $\langle . \rangle$ denotes spatial averaging and $\varepsilon(t) = \langle \varepsilon(\mathbf{x},t)\rangle$ is the time dependent but spatially averaged dissipation rate, $\Delta\tau$ is the time lag between the beginning of the air injection (wave impact) and the time of

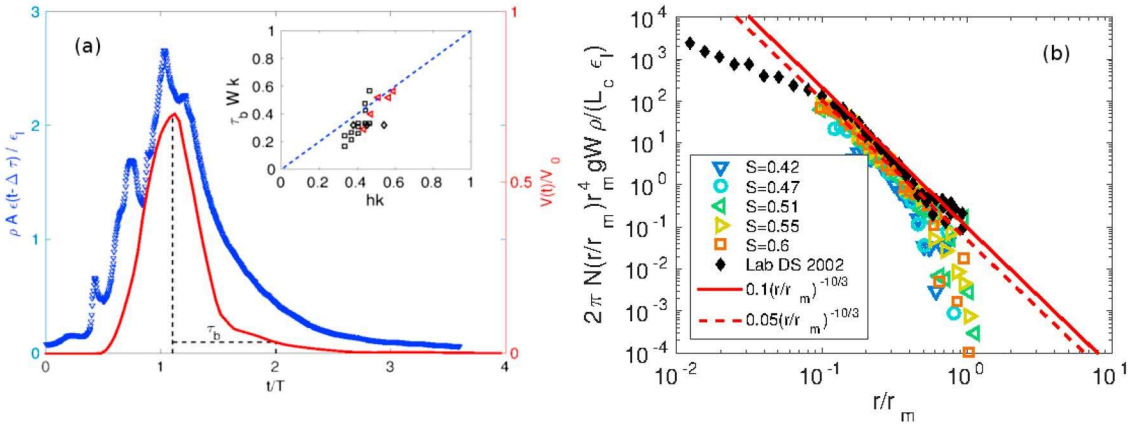

Figure 1. (a) An example of the time evolution (time normalized by the wave period t/T) of the volume of air entrained normalized by its maximum, $V(t)/V_0$, and the normalized turbulent dissipation rate, $\rho A\varepsilon(t-\Delta\tau)/\epsilon_l$, under a breaking wave in our numerical simulation [see *Deike et al.*, 2016, Figure 7] (main figure). $\Delta\tau$ is the time lag between the impact of the plunging jet and the maximum dissipation. The breaking time τ_b is indicated and corresponds to the time when $V(t)$ is just 10% of its maximum value. Figure 1a (inset) shows normalized breaking time, or bubble plume time τ_b, as a function of wave slope, for the simulations of *Deike et al.* [2016] (triangles) and laboratory experiments from *Callaghan et al.* [2013] (squares) and *Lamarre and Melville* [1991] (diamond). The weighted velocity in the experiments has been estimated following *Deike et al.* [2016]. A linear trend $\tau_b Wk = a(hk)$ (dashed line) is observed, with $a = 1$ a nondimensional constant. (b) Normalized time-averaged bubble size distribution, following equation (2). Color symbols are DNS data for various slopes, and black diamonds are the laboratory data from *Deane and Stokes* [2002] [see *Deike et al.*, 2016, Figure 13].

maximum dissipation, W is a dissipation-weighted vertical velocity that describes the buoyant rise of the bubble plume, r is the bubble radius, r_m is the maximum bubble radius, and B is the dimensionless bubble cloud constant. Note that the linear relationship between the bubble size distribution and $A = \pi h^2/4$ the cross sectional comes from the observation that the bubble cloud scales geometrically with h^2, i.e., both the penetration depth and the horizontal extent of the bubble cloud scale with h. The relationship equation (1) shows that the time evolution of the air entrained by the bubble plume is, to a good approximation, fully described by the time evolution of the dissipation rate.

The breaking time, or bubble plume time τ_b, is defined in Figure 1a, as the time for the plume to decay from its maximum value to 10% of it. The bubble time can also be defined as the characteristic exponential decay time of the volume [*Lamarre and Melville*, 1991], which gives a similar result. This definition appears consistent with the one used in *Callaghan et al.* [2013]. We find a relationship between the breaking time, τ_b, the wave height at breaking, h, and the dissipation-weighted velocity, W, $\tau_b W \propto h$, for both the laboratory data from *Callaghan et al.* [2013] and *Lamarre and Melville* [1991] and our numerical data [*Deike et al.*, 2016] (inset of Figure 1a).

Averaging $N(r, t)$ over the breaking time τ_b, we have

$$\bar{N}(r) = B\frac{1}{2\pi}\frac{L_c\epsilon_l}{\rho W g}r^{-10/3}r_m^{-2/3}, \tag{2}$$

with $\epsilon_l = \rho A\bar{\varepsilon}$ the dissipation rate per unit length of breaking crest, ρ the density, and $\bar{\varepsilon}$ the space and time-averaged dissipation rate over the active breaking event. The rescaled bubble size distribution $\bar{N}(r)$ for available laboratory and numerical data is shown in Figure 1b, providing an estimate of the bubble cloud constant, $B = 0.1 \pm 0.05$.

The total volume of entrained air during the breaking process is obtained by integrating the bubble size distribution over all radii. The time-dependent volume is

$$V(t) = \int_0^{r_m}(4\pi/3)r^3N(r,t)\mathrm{d}r = B\frac{\pi h^2 L_c}{4}\frac{\varepsilon(t-\Delta\tau)}{Wg}, \tag{3}$$

and the time-averaged volume is (with the dissipation rate per unit length of breaking crest being $\epsilon_l = b\rho c^5/g$)

$$\bar{V} = \int_0^{r_m}(4\pi/3)r^3\bar{N}(r)\mathrm{d}r = B\frac{\epsilon_l L_c}{\rho W g} = Bb\frac{L_c c^5}{Wg^2}. \tag{4}$$

Recall that the breaking strength b is physically related to the wave slope hk by $b \propto (hk)^{5/2}$, and by including a breaking threshold, *Romero et al.* [2012] showed that the dissipation by breaking for all available laboratory data can be described by $b = 0.4(S - 0.08)^{5/2}$.

2.2. Upscaling to the Open Ocean Using the Measured Breaking Statistics $\Lambda(c)$

We now define the volume flux of entrained air per unit area of ocean surface, per unit time, V_A, which has units of volume per unit area per unit time, i.e., velocity. Note that while V_A has dimensions of velocity, it should not be confused with the gas transfer velocity, since all bubbles do not fully dissolve in the water column. Following the framework of *Phillips* [1985], we compute V_A by integrating the volume of air, per unit length of breaking crest, entrained by breakers moving at a velocity between c and $c + \mathrm{d}c$, denoted by $v_l(c)$, over all breaking events, described by the distribution of length of breaking crest $\Lambda(c)$:

$$V_A = \int v_l(c)\Lambda(c)\mathrm{d}c. \tag{5}$$

By definition, $v_l(c)$ is related to the volume described in equation (4), $\bar{V}$, by

$$v_l(c) = \bar{V}/(L_c\tau_b), \tag{6}$$

where τ_b, defined previously for a single breaking wave, is the active breaking time or plume time.

The dispersion relation for deep water gravity waves is $c = \sqrt{g/k}$, and the breaking time τ_b, as shown in Figure 1, is $W = h/\tau_b$, leading to

$$V_A = \int B\frac{b}{(hk)}\frac{c^3}{g}\Lambda(c)\mathrm{d}c. \tag{7}$$

The volume flux of air entrained by breaking waves is therefore given by the third moment of $\Lambda(c)$, modulated by a factor that depends on the breaking strength and the associated dissipation, as well as the ratio of work done by buoyancy forces and mechanical dissipation, represented by the constant $B = 0.1$. The inertial scaling argument from *Drazen et al.* [2008] gives $b = \chi(hk)^{5/2}$, where χ is an order 1 nondimensional constant (the threshold will be introduced later). This leads to

$$V_A = \int B\chi(hk)^{3/2}\frac{c^3}{g}\Lambda(c)\mathrm{d}c. \tag{8}$$

Therefore, to estimate V_A, we need field measurements of the breaking statistics $\Lambda(c)$, together with measurements of the wave spectrum and the associated wave slope to compute $b/hk = \chi(hk)^{3/2}$. Note that equation (8) is a general formula that can be used for any wave state, in the presence of swell and wind waves, since it is based on a general representation of the wave and wave breaking statistics.

2.3. Estimating $v_l(c)$ Using Field Measurements of Surface Waves and Wave Breaking

Romero et al. [2012], followed by *Sutherland and Melville* [2013, 2015], showed that to properly close the wave breaking energy budget in the ocean, we need to consider spectral properties of the wavefield and compute a spectral breaking parameter $b(c)$, using the wave spectrum (and wave slope spectrum), measured by high-resolution wave data. This was shown by comparing a measure of the dissipation using the fifth moment of $\Lambda(c)$, using wave spectral measurements for $b(c)$, to measurements of the subsurface turbulence created by breaking, [*Sutherland and Melville*, 2013, 2015]. We follow this path to perform a spectral estimate of the quantity b/hk. Following *Romero et al.* [2012], the spatially integrated omnidirectional wave spectrum, $\phi(k)$, is measured in the field and the saturation spectrum is defined as $B(k) = \phi(k)k^3$. Figure 2a shows an example of a wave spectrum $\phi(k)$ measured during the HIRES 2010 experiment, from an aircraft, using a topographic lidar as described in *Lenain and Melville* [2017], together with the associated saturation spectrum, $B(k)$, both extrapolated at higher frequencies (following *Romero et al.* [2012] and consistent with recent observations from *Melville et al.* [2016]). The spectrum shows a $\phi(k) \propto k^{-2.5}$ power law at low wave numbers, before a transition to saturation, $\phi(k) \propto k^{-3}$, at higher wave numbers (see *Melville et al.* [2016] for a complete discussion on the transition from equilibrium to saturation spectra).

We now perform a "spectral estimate" of $b/hk = \chi(hk)^{3/2}$, from the wave spectrum data. The spectral breaking parameter, as defined by *Romero et al.* [2012], is given by $b(k) = A_1(B(k)^{1/2} - B_T^{1/2})^{5/2}$, with B_T and A_1 coefficients computed by *Romero et al.* [2012] to balance wind input and dissipation by breaking in a spectral wave model, consistent with the laboratory experiments and numerical simulations of breaking waves, and used in *Sutherland and Melville* [2013, 2015]. The spectral slope is given by $hk = B(k)^{1/2}$. We consider

$$b/hk = A_1(B(k)^{1/2} - B_T^{1/2})^{3/2} \tag{9}$$

Figure 2b shows the distribution of length of breaking crests, $\Lambda(c)$, obtained from airborne visible imagery. The distribution reaches its maximum around 2 m/s, and rolls off for smaller velocities. It follows a trend close

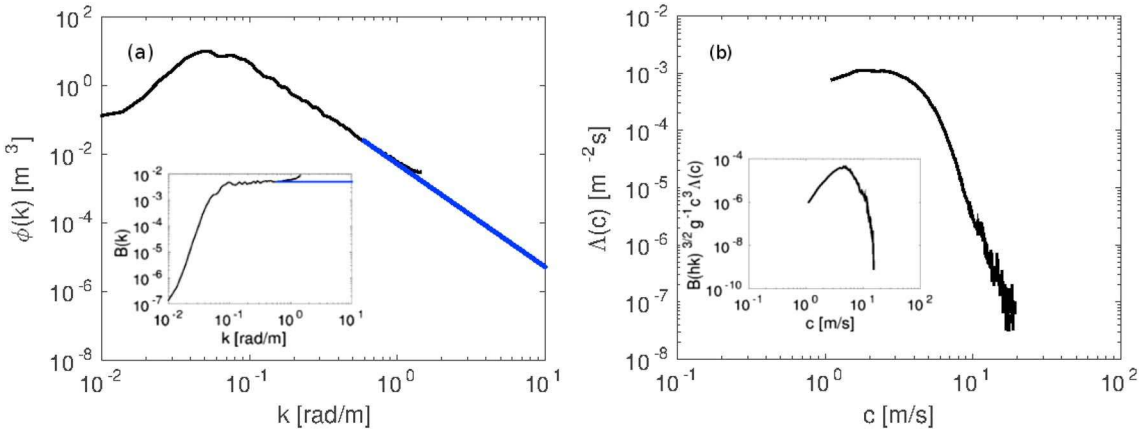

Figure 2. (a) Measured omnidirectional wave spectrum $\phi(k)$ from airborne data, with the extrapolated tail of the saturation spectrum (main figure). Figure 2a shows corresponding saturation spectrum $B(k)$ (inset). The spectral slope and the spectral breaking parameter are estimated from $B(k)$. (b) $\Lambda(c)$ for the same data from airborne video imagery (main figure). Figure 2b shows integrand of the volume flux of air, $v_l(c) = B\frac{b}{(hk)}\frac{c^3}{g}\Lambda(c)$, as a function of the speed of the breaking crest c (inset). It corresponds to the third moment of $\Lambda(c)$, modulated by b/hk, estimated spectrally using equation (9).

to c^{-6} from 2 to 10 m/s, as described in earlier work [*Kleiss and Melville*, 2010; *Sutherland and Melville*, 2013] and predicted by *Phillips* [1985]. The third moment of $\Lambda(c)$, modulated by b/hk, i.e., $v_l(c)$, is shown as an inset in Figure 2b. It corresponds to an estimate of the volume of entrained air for breakers with speeds between c and $c + dc$. The maximum contribution to the air entrainment is around $c = 3$–4 m/s, corresponding to wavelengths of approximately 6 to 10 m. Parameterization of $\Lambda(c)$ is challenging [*Sutherland and Melville*, 2013], which makes measurements of $\Lambda(c)$ very valuable to estimate the role of breaking waves in upper ocean processes; therefore, in the following, we use the measured data of $\Lambda(c)$ to compute the entrained air rather than a model.

3. Ocean Estimate of V_A Using Wave and Breaking Statistics

We now use equation (8) to estimate the volume flux of air entrained by breaking waves in the open ocean, using field measurements of the spectral estimate of b/hk (equation (9)), and the distribution of length of breaking crests, $\Lambda(c)$, from video and infrared imagery. We use data sets collected previously and described in earlier publications: airborne data from the GOTEX 2004 experiment [*Kleiss and Melville*, 2010; *Romero and Melville*, 2010; *Romero et al.*, 2012] and the HIRES 2010 experiment [*Lenain and Melville*, 2017], as well as video data taken from R/P FLIP during the RaDyo 2009, SoCal 2010, and HIRES 2010 experiments [*Sutherland and Melville*, 2013, 2015].

For the data taken from R/P FLIP, we use measurements of $\Lambda(c)$ both from visible and infrared cameras. We consider breaking waves that entrain air, only keeping speeds above 2 m/s. Infrared cameras also measure the temperature signatures of breaking waves that do not entrain air (typically with speeds below 1–2 m/s); therefore, we only consider the "visible" part of the $\Lambda(c)$ distribution for our analysis, since we are interested in an estimate of the air entrainment. This is done by applying a threshold, $\Lambda_v(c)$: any value of $\Lambda(c)$ above $\Lambda_v(c)$ is replaced by $\Lambda_v(c)$. The threshold is chosen to be $\Lambda_v(c) = 2 \cdot 10^{-3}$ s/m^2, corresponding to an average of the observed maximum values of $\Lambda(c)$ from the visible measurements of *Kleiss and Melville* [2010], *Zappa et al.* [2012], *Sutherland and Melville* [2013], and *Gemmrich et al.* [2013] and chosen to minimize the differences in the estimated V_A from visible and infrared data when both measurements are available at the same time (i.e., for some data from *Sutherland and Melville* [2013]). Changing this threshold obviously changes the estimate of the volume, and the variability to the procedure is included in the error bars presented below, and is the largest source of uncertainty in our procedure. The other main source of uncertainty regards the measurement of $\Lambda(c)$ itself which is challenging to perform, both from airborne or research vessels and platforms. As pointed out earlier, we use the measured data of $\Lambda(c)$ to compute the volume flux V_A. The error in the measurements of the wave spectrum should be negligible compared to the one for $\Lambda(c)$ when computing V_A.

Combining the spectral estimate of the wave slope term and the $\Lambda(c)$ distribution provides a scale-by-scale estimate of the strength and occurrence of breaking waves. Therefore, it provides the required representation

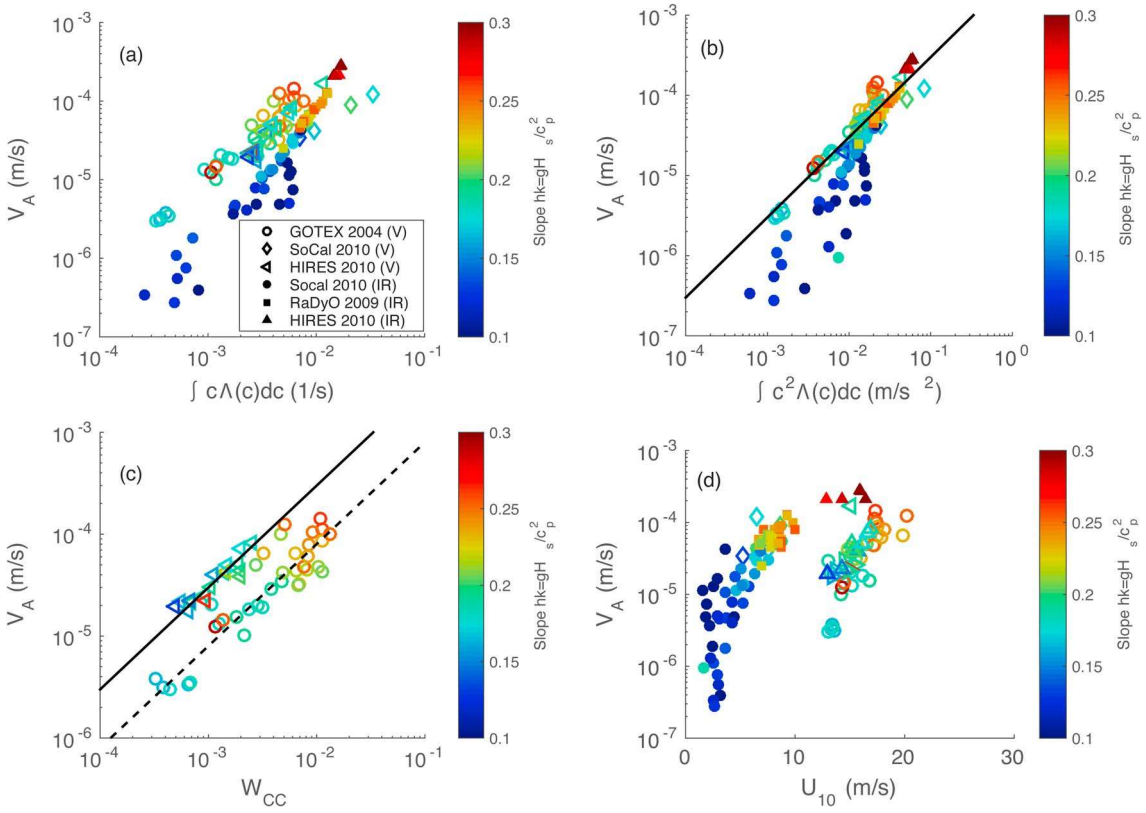

Figure 3. Total volume flux of air entrained by breaking waves, V_A (equation (8)) as a function of oceanographic and meteorological parameters. (a, b) V_A as a function of the integrated first (Figure 3a) and second (Figure 3b) moments of $\Lambda(c)$. The solid black line is $V_A = \zeta \int c^2 \Lambda(c) dc$ a linear least squares fit for $V_A > 10^{-6}$ m/s, with $\zeta = 3 \pm 1 \cdot 10^{-3}$ 1/s. (c) V_A as a function of the active whitecap coverage W_{CC}. The solid black line is $V_A = \iota_1 W_{CC}$, and the dashed line is $V_A = \iota_2 W_{CC}$, from least squares linear fits to the two data sets, with $\iota_1 = 3 \pm 1 \cdot 10^{-3}$ m/s and $\iota_2 = 8 \pm 3 \cdot 10^{-3}$ m/s. (d) V_A as a function of the wind speed at 10 m. No clear relationship is visible. Color code is the global wave slope gH_s/c_p^2. Open symbols correspond to measurements of $\Lambda(c)$ with visible imagery: circles for GOTEX 2004, diamonds for SoCal 2010, and triangles for HIRES 2010. Filled symbols correspond to measurements of $\Lambda(c)$ with infrared imagery, cut to keep only the visible part of the distribution: circles for SoCal 2010, triangles for HIRES 2010, and squares for RaDyO 2009.

of the ocean-wave state, motivating a discussion of the estimate of the volume V_A of air entrained by breaking waves as a function of lower moments of $\Lambda(c)$, and various oceanographic parameters.

Figures 3a and 3b show V_A as a function of the first (a) and second (b) moments of $\Lambda(c)$. In both cases, a correlation is observed between the quantities, which can be expected since the distribution $\Lambda(c)$ approximately follows a $\Lambda(c) \propto c^{-6}$ relationship for some ranges of larger c. Scatter between the different data sets is visible between the first moment and V_A, while a relatively good linear relation is observed between the second moment and V_A, for volumes of air above a certain threshold (between 10^{-6} and 10^{-5} m/s depending on the data set). The data below this threshold correspond to wave states with weak air entrainment and small global wave slope gH_s/c_p^2, where H_s is the significant wave height and c_p the phase speed at the peak of the wave spectrum (or the weighted phase speed in the presence of swell) [see *Sutherland and Melville*, 2013, 2015]. Note that some studies on ocean-atmosphere interactions have used the wind speed peak velocity when defining the wave age [*Toba et al.*, 2006; *Zhao et al.*, 2006]. Note also that the values of V_A between 10^{-3} and 10^{-6} m/s appear compatible with measurements of the void fraction just below the surface [*Terrill et al.*, 2001].

Figure 3c shows the volume flux of air, V_A, as a function of the active whitecap coverage W_{CC}, defined as the percentage area of sea surface covered by actively breaking whitecaps (see *Kleiss and Melville* [2010, 2011], *Lenain and Melville* [2017], and *Melville et al.* [2016] for details on how W_{CC} is computed). For each data set, a reasonable linear correlation is visible. This is the first rational model that demonstrates a relationship between the active whitecap coverage and the air entrainment. The differences between the data sets are probably related to the differences in defining and computing W_{CC}, for different field and light conditions. Therefore, the particular values of the fitted constants should be considered carefully. Note that we observe more scatter in the correlation between V_A and the whitecap coverage W_{CC} than between V_A and the second moment of $\Lambda(c)$.

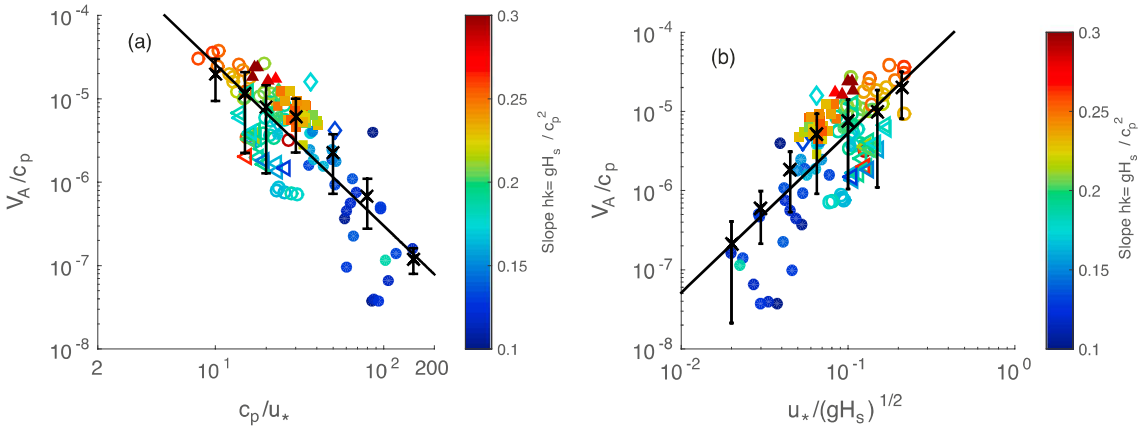

Figure 4. (a) V_A/c_p as a function of wave age, c_p/u_*. The solid black line is a least squares fit, $V_A = \chi_1(c_p/u_*)^{-\xi_1}$, with $\chi_1 = 2.3 \pm 3 \cdot 10^{-3}$ and $\xi_1 = 1.9 \pm 0.3$ fitted nondimensional coefficients. The black crosses are bin-averaged data. (b) V_A/c_p as a function of the ratio of the friction velocity to the ballistic velocity, $u_*/\sqrt{gH_s}$. The solid black line is a least squares fit, $V_A/c_p = \chi_2(u_*/\sqrt{gH_s})^{\xi_2}$, with $\chi_2 = 5.4 \pm 5 \cdot 10^{-4}$ and $\xi_2 = 2 \pm 0.3$ fitted nondimensional coefficients. The black crosses are bin-averaged data. Color code is the wave slope, and symbol key is the same as in Figure 3.

Both quantities are related to the active area of breaking waves, but the intrinsic definition of $\Lambda(c)$ permits a more consistent comparison between data sets.

Figure 3d shows the volume flux of air, V_A, as a function of wind speed at 10 m, U_{10}, and no clear relationship can be observed. This result is of considerable importance since most of the current gas transfer parameterizations are based on the wind speed with no dependance on the wave state nor breaking. Our results show clearly that the wind speed alone does not describe the entrainment of air. For the same wind speed, we get differences of more than 2 orders of magnitude in the amount of air entrained, depending on the wave conditions. Furthermore, wind speeds varying by more than a factor 4 can give the same volume of entrained air.

Figure 4a shows the total volume flux of air entrained, rescaled by the peak velocity, V_A/c_p, as a function of wave age, c_p/u_*, where u_* is the friction velocity. The volume of entrained air decreases with the wave age, which corresponds to younger seas presenting more and stronger breaking events and therefore entraining more air. The bin-averaged data clearly show this decreasing trend, close to a power law. While some scatter remains between the different data sets, we observe a power law trend, $V_A = \chi_1(c_p/u_*)^{-\xi_1}$. The fitted nondimensional coefficients are the exponent, $\xi_1 = 1.9 \pm 0.3$, and the coefficient $\chi_1 = 2.3 \pm 3 \cdot 10^{-3}$. Figure 4b shows V_A/c_p as a function of the friction velocity rescaled by the ballistic velocity $\sqrt{gH_s}$ [*Drazen et al.*, 2008]. The volume increases with $u_*/\sqrt{gH_s}$ as expected, and we observe a similar power law trend on the bin-averaged data. The data are described by $V_A/c_p = \chi_2(u_*/\sqrt{gH_s})^{\xi_2}$, with again some scatter between the various data sets. The fitted exponent for the power law is $\xi_2 = 2 \pm 0.3$, and the coefficient $\chi_1 = 5.4 \pm 5 \cdot 10^{-4}$. Note that the two exponents for the power laws, $\xi_1 \approx \xi_2$, are consistent with the fetch-limited relationship $c_p \propto \sqrt{gH_s}$.

Note that the increased scatter visible for older wave ages (large c_p/u_*), or small $u_*/\sqrt{gH_s}$, is explained by the fact that fewer breaking events are present, leading to a smaller sampling size when measuring the breaking statistics $\Lambda(c)$ and therefore leading to more scatter in the data.

While some scatter between the data sets is still present, these rescaled plots show that a combination of wind and wave variables permits a better description of the volume of entrained air, with an overall scatter in the data significantly reduced compared to the relationship where the wind only was considered. The remaining scatter in the data is of the same order of magnitude as that when rescaling $\Lambda(c)$ alone in *Sutherland and Melville* [2013].

4. Discussion

We have presented a rational model to estimate the volume flux of air entrained by breaking waves in the ocean. We have shown that the volume flux of air V_A entrained by breaking waves (volume per unit area per unit time: the air entrainment velocity) is described by the third moment $\Lambda(c)$, modulated by a function of the wave slope, which extends the work of *Phillips* [1985], by completing the physical interpretation of the

moments of $\Lambda(c)$ from the first to the fifth. Our formulation is general and is not limited to any particular wave state. We obtain air entrainment velocities, V_A, between 10^{-6} and 10^{-4} m/s, which appear compatible with existing limited measurements of the void fraction below the surface. From V_A, we can estimate the total surface area of bubbles entrained by breaking waves from the bubble size distribution, by assuming minimum and maximum bubble sizes. The obtained increase in the exchange area due to the entrained bubbles is at least 10% and up to 50% (this number is sensitive to the chosen boundaries of the bubble size distribution and of course to the error bars on V_A). These numbers are very significant, showing that even if breaking is intermittent in space and time, it is an essential ingredient for air-sea interaction, in particular for gas transfer. Moreover, the pressure acting on the bubbles entrained in the water column is increased by hydrostatic pressure and surface tension. Because of this compression effect, gas is forced into solution, leading to a large increase in the transfer and saturation of gases. Clean bubbles may eventually fully dissolve in the water [*Woolf and Thorpe*, 1991; *Keeling*, 1993; *Liang et al.*, 2012, 2013].

The volume flux of air, V_A, presents a strong linear correlation with the second moment of the breaking statistics, $\int c^2\Lambda(c)$. A reasonable linear correlation between V_A and the active whitecap coverage is also observed, and we believe that some of the observed scatter is due to the nonuniformity in the way the whitecap coverage is measured. No clear relationship between the wind speed at 10 m, U_{10}, and V_A is observed, which can be easily explained by the fact that a given wind speed does not correspond to a unique wave state, except perhaps in the asymptotic case of "fully developed" waves, but that is the exception [*Hanley et al.*, 2010]. Better correlations are observed with parameters depending both on the wave conditions and the wind, such as the wave age c_p/u_*, or the friction velocity rescaled by the ballistic velocity $u_*/\sqrt{gH_s}$. A similar discussion has recently been presented independently by *Liang et al.* [2017]. Inspired by these results, we find the following relationships, $V_A/c_p = \chi_1(c_p/u_*)^{-\xi_1}$, and $V_A/c_p = \chi_2(u_*/\sqrt{gH_s})^{\xi_2}$, with $\xi_1 \approx \xi_2 \approx 1.9 \pm 0.3$, and $\chi_1 = 2.3 \pm 3 \cdot 10^{-3}$, $\chi_2 = 5.4 \pm 5 \cdot 10^{-4}$ fitted nondimensional constants. More field measurements are needed to reduce the error bars and clarify wether the observed scatter comes from differences in measurements and data processing or if other wave and meteorological parameters have to be considered to properly rescale the data.

To conclude, we believe that these relationships could serve as the basis for future gas transfer parameterizations and that this work opens the way for physical parameterization of gas transfer due to bubbles entrained by breaking waves.

Acknowledgments
We thank Laurent Grare, Nick Pizzo, Leonel Romero, and Peter Sutherland for their helpful discussions. This work was funded by grants to W.K.M. by NSF (OCE-1634289) and ONR (Physical Oceanography-N00014-15-1-25-29). Data used in this paper have been collected during several field experiments, have been published in previous work, and are available upon request.

References

Callaghan, A. H., G. B. Deane, and D. M. Stokes (2013), Two regimes of laboratory whitecap foam decay: Bubble-plume controlled and surfactant stabilized, *J. Phys. Oceanogr.*, *43*, 1114–1126.
de Leeuw, G., E. L. Andreas, M. D. Anguelova, C. W. Fairall, E. R. Lewis, C. O'Dowd, M. Schulz, and S. E. Schwartz (2011), Production flux of sea spray aerosol, *Rev. Geophys.*, *49*, RG2001, doi:10.1029/2010RG000349.
Deane, G., and M. Stokes (2002), Scale dependance of bubble creation mechanisms in breaking waves, *Nature*, *418*, 839–844.
Deike, L., S. Popinet, and W. Melville (2015), Capillary effects on wave breaking, *J. Fluid Mech.*, *769*, 541–569.
Deike, L., W. Melville, and S. Popinet (2016), Air entrainment and bubble statistics in breaking waves, *J. Fluid Mech.*, *801*, 91–129.
Derakhti, M., and J. T. Kirby (2016), Breaking-onset, energy and momentum flux in unsteady focused wave packets, *J. Fluid Mech.*, *790*, 553–581.
Drazen, D. A., W. K. Melville, and L. Lenain (2008), Inertial scaling of dissipation in unsteady breaking waves, *J. Fluid Mech.*, *611*(1), 307–332.
Duncan, J. (1981), An experimental investigation of breaking waves produced by a towed hydrofoil, *Proc. R. Soc. A*, *377*(1770), 331–348.
Garbe, C. S., et al. (2014), *Transfer Across the Air-Sea Interface*, pp. 55–112, Springer, Berlin.
Gemmrich, J., C. J. Zappa, M. L. Banner, and R. P. Morison (2013), Wave breaking in developing and mature seas, *J. Geophys. Res. Oceans*, *118*, 4542–4552, doi:10.1002/jgrc.20334.
Grare, L., W. L. Peirson, H. Branger, J. W. Walker, J.-P. Giovanangeli, and V. Makin (2013), Growth and dissipation of wind-forced, deep-water waves, *J. Fluid Mech.*, *722*, 5–50.
Hanley, K. E., S. E. Belcher, and P. P. Sullivan (2010), A global climatology of wind-wave interaction, *J. Phys. Oceanogr.*, *40*(6), 1263–1282.
Keeling, R. F. (1993), On the role of large bubbles in air-sea gas exchange and supersaturation in the ocean, *J. Mar. Res.*, *51*(2), 237–271.
Kleiss, J. M., and W. K. Melville (2010), Observations of wave breaking kinematics in fetch-limited seas, *J. Phys. Oceanogr.*, *40*(12), 2575–2604.
Kleiss, J. M., and W. K. Melville (2011), The analysis of sea surface imagery for whitecap kinematics, *J. Atmos. Oceanic Technol.*, *28*(2), 219–243.
Lamarre, E., and W. Melville (1991), Air entrainment and dissipation in breaking waves, *Nature*, *351*, 469–472.
Lenain, L., and W. Melville (2017), Evidence of sea-state dependence of aerosol concentration in the marine atmospheric boundary layer, *J. Phys. Oceanogr.*, *47*, 69–84.
Liang, J.-H., J. McWilliams, P. Sullivan, and B. Baschek (2012), Large eddy simulation of the bubbly ocean: New insights on subsurface bubble distribution and bubble-mediated gas transfer, *J. Geophys. Res.*, *117*, C04002, doi:10.1029/2011JC007766.
Liang, J.-H., C. Deutsch, J. C. McWilliams, B. Baschek, P. P. Sullivan, and D. Chiba (2013), Parameterizing bubble-mediated air-sea gas exchange and its effect on ocean ventilation, *Global Biogeochem. Cycles*, *27*, 894–905, doi:10.1002/gbc.20080.
Liang, J.-H., S. R. Emerson, E. A. D'Asaro, C. L. McNeil, R. R. Harcourt, P. P. Sullivan, B. Yang, and M. F. Cronin (2017), On the role of sea-state in bubble-mediated air-sea gas flux during a winter storm, *J. Geophys. Res. Oceans*, *122*, doi:10.1002/2016JC012408.

Lim, H.-J., K.-A. Chang, Z.-C. Huang, and B. Na (2015), Experimental study on plunging breaking waves in deep water, *J. Geophys. Res. Oceans*, *120*, 2007–2049, doi:10.1002/2014JC010269.
Melville, W. K. (1996), The role of surface wave breaking in air-sea interaction, *Annu. Rev. Fluid Mech.*, *28*, 279–321.
Melville, W. K., and A. V. Fedorov (2015), The equilibrium dynamics and statistics of gravity-capillary waves, *J. Fluid Mech.*, *767*, 449–466.
Melville, W. K., L. Lenain, D. R. Cayan, M. Kahru, J. Kleissl, P. Linden, and N. Statom (2016), The modular aerial sensing system, *J. Atmos. Oceanic Technol.*, *33*(6), 1169–1184.
Phillips, O. (1985), Spectral and statistical properties of the equilibrium range in wind-generated gravity waves, *J. Fluid Mech.*, *156*(1), 505–531.
Romero, L., and W. K. Melville (2010), Airborne observations of fetch-limited waves in the Gulf of Tehuantepec, *J. Phys. Oceanogr.*, *40*(3), 441–465.
Romero, L., W. K. Melville, and J. M. Kleiss (2012), Spectral energy dissipation due to surface wave breaking, *J. Phys. Oceanogr.*, *42*, 1421–1441.
Sutherland, P., and W. K. Melville (2013), Field measurements and scaling of ocean surface wave-breaking statistics, *Geophys. Res. Lett.*, *40*, 3074–3079, doi:10.1002/grl.50584.
Sutherland, P., and W. K. Melville (2015), Field measurements of surface and near-surface turbulence in the presence of breaking waves, *J. Phys. Oceanogr.*, *45*, 943–966.
Taylor, G. I. (1935), Statistical theory of turbulence, *Proc. R. Soc. A*, *151*(873), 421–444.
Terrill, E. J., W. K. Melville, and D. Stramski (2001), Bubble entrainment by breaking waves and their influence on optical scattering in the upper ocean, *J. Geophys. Res.*, *108*, 16,815–16,823.
Toba, Y., S. Komori, Y. Suzuki, and D. Zhao (2006), Similarity and dissimilarity in air–sea momentum and CO_2 transfers: The nondimensional transfer coefficients in light of windsea Reynolds number, *Atmos. Ocean Interact.*, *2*, 53–82.
Veron, F. (2015), Ocean spray, *Annu. Rev. Fluid Mech.*, *47*, 507–538.
Wallace, D., and C. Wirick (1992), Large air–sea gas fluxes associated with breaking waves, *Nature*, *356*, 694–696.
Woolf, D. K., and S. Thorpe (1991), Bubbles and the air-sea exchange of gases in near-saturation conditions, *J. Mar. Res.*, *49*(3), 435–466.
Zappa, C. J., M. Banner, H. Schultz, J. Gemmrich, R. Morison, D. LeBel, and T. Dickey (2012), An overview of sea state conditions and air-sea fluxes during RaDyO, *J. Geophys. Res.*, *117*, C00H19, doi:10.1029/2011JC007336.
Zhao, D., Y. Toba, K.-I. Sugioka, and S. Komori (2006), New sea spray generation function for spume droplets, *J. Geophys. Res.*, *111*, C02007, doi:10.1029/2005JC002960.